

## Porous carbon nanofiber–sulfur composite electrodes for lithium/sulfur cells†

Liwen Ji,<sup>‡a</sup> Mumin Rao,<sup>‡§b</sup> Shaul Aloni,<sup>a</sup> Lei Wang,<sup>b</sup> Elton J. Cairns<sup>b</sup> and Yuegang Zhang<sup>\*a</sup>

Received 1st August 2011, Accepted 21st September 2011

DOI: 10.1039/c1ee02256c

Sulfur (S) encapsulated in porous carbon nanofibers (CNFs) was synthesized *via* electrospinning, carbonization and solution-based chemical reaction–deposition method. The chemical reaction–deposition strategy provides intimate contact between the S and the CNFs. This would not necessarily be the case for other reported methods, such as ball milling and thermal treatment. These novel porous carbon nanofiber–sulfur (CNF–S) nanocomposites with various S loadings showed high reversible capacity, good discharge capacity retention and enhanced rate capability when they were used as cathodes in rechargeable Li/S cells. We demonstrated here that an electrode prepared from a porous CNF–S nanocomposite with 42 wt% S maintains a stable discharge capacity of about 1400 mA h g<sup>−1</sup> at 0.05 C, 1100 mA h g<sup>−1</sup> at 0.1 C and 900 mA h g<sup>−1</sup> at 0.2 C. We attribute the good electrochemical performance to the high electrical conductivity and the extremely high surface area of the CNFs that homogeneously disperse and immobilize S on their porous structures, alleviating the polysulfide shuttle phenomenon. SEM measurements showed that the porous CNF structures remained nearly unchanged even after 30 cycles' discharging/charging at 0.05 C.

### Introduction

Lithium (Li) secondary cells have become one of the most important and efficient devices for storage of electrical energy generated from renewable sources such as solar and wind. A breakthrough in novel electrochemically active materials and new redox concepts is still urgently required to create future

batteries with dramatically increased energy/power density to meet the requirements of large-scale energy storage devices.<sup>1–6</sup>

Sulfur (S) is a promising electrode material for Li secondary cells and has attracted attention due to its high theoretical specific capacity of 1675 mA h g<sup>−1</sup> and high theoretical specific energy (with a Li electrode) of about 2600 Wh kg<sup>−1</sup>.<sup>7–17</sup> In addition, S is inexpensive, abundant, non-toxic and environmentally benign.<sup>7–17</sup> Therefore, Li/S cells have the potential to replace most other rechargeable Li cells.<sup>7–17</sup> Unfortunately, the Li/S cell still faces several serious challenges, including low utilization of active material (S), low coulombic efficiency and rapid capacity loss on repeated discharging/charging. These problems are traceable to the low electronic conductivity (insulating nature) and the high tendency to dissolve in organic solvent-based electrolytes of the long chain polysulfide ions which are formed during the continuous discharge/charge processes, and the accompanying “shuttle” phenomenon, which

<sup>a</sup>The Molecular Foundry, Lawrence Berkeley National Laboratory, Berkeley, California, 94720, USA. E-mail: yzhang5@lbl.gov

<sup>b</sup>Environmental Energy Technologies Division, Lawrence Berkeley National Laboratory and Department of Chemical & Biomolecular Engineering, University of California, Berkeley, CA, 94720, USA

† Electronic supplementary information (ESI) available. See DOI: 10.1039/c1ee02256c

‡ These authors contributed equally to this work.

§ Visiting researcher from College of Materials Science and Engineering, South China University of Technology, Guangzhou 510641, China.

### Broader context

Compared with conventional lithium ion cells, the lithium/sulfur cell has much higher theoretical specific capacity and specific energy. Considering the abundance of sulfur, the rechargeable lithium/sulfur cell should have great potential for low-cost electrical vehicles and grid-scale energy storage applications. To meet the requirement of long cycle life and high rate performance, however, there is an urgent need to develop a novel and nanostructured sulfur electrode that can overcome the intrinsic limitations of bulk sulfur electrodes, which include the insulating nature of elemental sulfur and the high solubility of the long chain polysulfide ions in the organic solvent-based electrolytes. In the current study, we employed a novel strategy to fabricate electrochemically active sulfur-decorated carbon nanofibers and evaluated their electrochemical behavior as electrodes in rechargeable lithium/sulfur cells using an ionic liquid-based electrolyte. It was demonstrated that the new nanocomposite sulfur electrode has high reversible capacity and improved cycle life, even at high discharge/charge rates.

results in corrosion of the Li and increases the internal resistance of the cell.<sup>7–13,16–25</sup>

The research and development efforts to enhance Li/S cell performance have been focused on, firstly, fabricating porous carbon–S nanocomposites<sup>10,11,13,16,18–20,26–32</sup> or preparing conducting polymer–S composites.<sup>33–35</sup> Here, the porous carbon and conductive polymer act as electronic conductor and absorbing agent to improve the electrical conductivity and to restrict the dissolution of polysulfides in the electrolytes at the same time. Secondly, using some alternative electrolyte (including mixed electrolytes), or electrolyte modifications (such as adding some ceramic nanoparticles, or additives to the electrolyte). Novel electrolytes such as room temperature ionic liquids which have wide electrochemical stability windows, low volatility, good thermal and chemical stabilities, and are also environmentally benign, can decrease the solubility of polysulfides, increase the ionic conductivity, and lower the viscosity at the same time.<sup>36–44</sup> The use of additives in the electrolyte (including electrolyte modifications) can enhance the ionic conductivity, mitigate the problem of polysulfides dissolving in electrolytes, and increase the interfacial compatibility with metallic Li.<sup>44–46</sup> Thirdly, using some new binders, which have high adhesion ability for bonding the electrode materials to the current collector, good ionic conductivity, as well as low solubility in the organic electrolytes result in a decrease in the cell resistance.<sup>47,48</sup>

In this work, we load elemental S into porous carbon nanofibers (CNFs) and prepare a porous carbon nanofiber–sulfur (CNF–S) composite electrode material for rechargeable Li/S cells (Fig. 1 shows a schematic diagram of the steps for synthesizing the porous CNF–S nanocomposite and evaluating the electrochemical performance of these nanocomposite-based cathodes in

rechargeable Li/S cells). Here, porous CNFs are prepared by the low cost, simple and environmentally benign electrospinning technique and the subsequent carbonization process, which have been popularly used to fabricate electrodes for lithium-ion batteries, fuel cells, *etc.*<sup>49–56</sup> The S is readily incorporated into the porous CNF's *via* the chemical solution reaction–deposition strategy using S-containing precursors.<sup>57</sup> The porous CNFs with high electronic conductivity and excellent mechanical strength can establish more intimate electronic contact between S and the current collector, and so improve S utilization. These linear, long, and interconnected porous CNFs with very high surface-to-volume ratios and various kinds of pore volumes (see Table S1 in the ESI†) can encapsulate a large amount of S in the pore structure. The porous CNF's can also play the role of strong absorbent to retain polysulfides and reduce their dissolution into the electrolyte. In addition, those porous CNFs provide an effective electronic conduction path and their network-like structure forms a stable structure of the S electrode.<sup>58</sup>

## Experimental procedures

### Chemicals

Polyacrylonitrile (PAN) (average  $M_w$  150 000, Aldrich), poly (methyl methacrylate) (PMMA) (average  $M_w$  120 000, Aldrich), *N,N*-dimethylformamide (DMF) (anhydrous, 99.8%, Aldrich), sodium sulfide ( $\text{Na}_2\text{S}$ ) (anhydrous, Alfa Aesar), sublimed S powder (99.9%, Mallinckrodt), formic acid ( $\text{HCOOH}$ ) (88%, Aldrich), *N*-methylpyrrolidone (NMP) (anhydrous, 99.5%, Aldrich), *N*-methyl-*N*-butylpyrrolidinium bis(trifluoromethanesulfonyl) imide ( $\text{PYR}_{14}\text{TFSI}$ ,  $\geq 98.0\%$ , Aldrich), poly(ethylene glycol) dimethyl

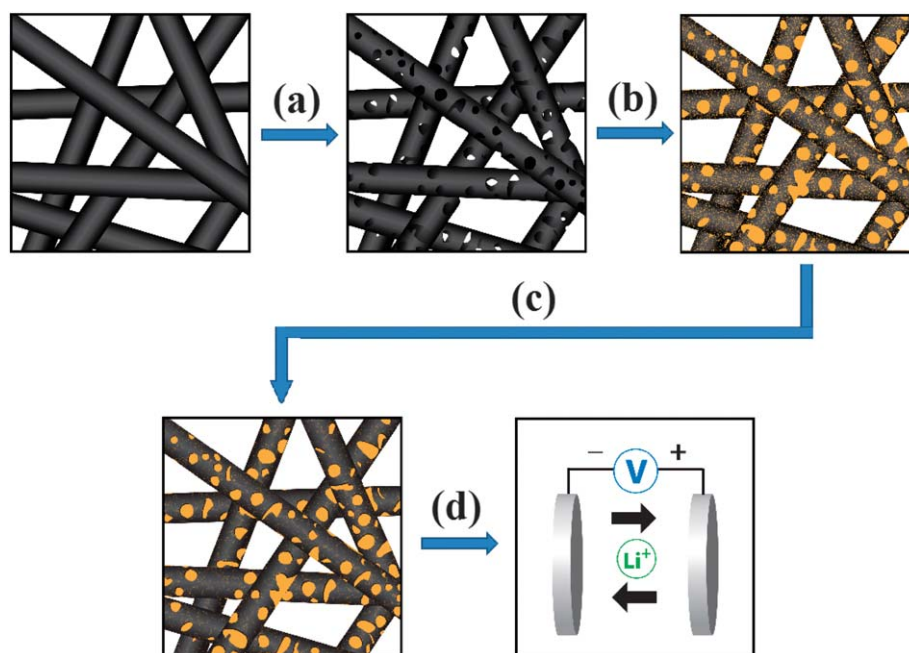


**Fig. 1** Schematic illustration of the experimental procedures. (a) Carbonizing electrospun PAN/PMMA bicomponent nanofibers to obtain porous CNFs; (b) incorporating S into the porous CNF nanostructure *via* solution-based chemical reactions to obtain porous CNF–S nanocomposites; (c) thermal treatment of the as-formed porous CNF–S nanocomposites to remove S outside of the pores; (d) assembling Li/S cells to evaluate the electrochemical performance of the thermally treated porous CNF–S nanocomposite electrodes.

ether (PEGDME,  $M_w = 250$ , Aldrich), and lithium bis(tri-fluoromethylsulfonyl)imide (LiTFSI, 99.95%, Aldrich) were used without further treatments.

### Preparation of PAN/PMMA nanofibers<sup>59</sup>

PAN and PMMA blends were prepared by dissolving 10 wt% total PAN/PMMA bicomponent polymers at a mass ratio of 1 : 1 in DMF solvent at 60 °C under constant stirring for at least 24 hours, followed by ultrasonic treatment (FS20H Sonicator, Fisher Scientific) for another 2 hours. Finally, strong mechanical stirring was applied for further 24 hours in order to obtain a homogeneous PAN/PMMA solution. A variable high voltage power supply (Gamma ES40P) was used to provide a high voltage (~12.5 kV) for electrospinning. The flow rate and tip-collector distance were fixed at 1 ml h<sup>-1</sup> and 15 cm, respectively. The positive terminal of the high voltage power supply was connected to the needle tip. The grounded electrode was connected to a metallic collector wrapped with aluminium (Al) foil. Dry nanofibers were accumulated on the collection plate as a fibrous web that was mechanically removed from the supporting Al foil.

### Preparation of porous CNFs

The carbonization of the PAN/PMMA precursor nanofiber webs was performed in an atmosphere-controlled tube furnace. First, the electrospun PAN/PMMA nanofibers were stabilized at 280 °C in air environment for 6 hours. In this process, thermoplastic PAN was converted to a non-plastic cyclic or ladder compound,<sup>49–56,59</sup> while PMMA melted.<sup>59</sup> The temperature was then increased from 280 °C to 1000 °C in high-purity argon (Ar) and held for 8 hours in order to complete the carbonization process.<sup>59</sup> In the PAN/PMMA blended nanofibers, PAN serves as the carbon precursor,<sup>49–56,59</sup> and PMMA acts as the pore generator.<sup>59</sup> PMMA phase-separates from PAN during electrospinning and decomposes to form pores during the carbonization of PAN. This procedure allows the direct elimination of PMMA during the PAN carbonization step, creating porous CNFs without the use of additional chemical treatment. As a result, the fabrication of these porous CNFs is simpler and faster than many other methods.

### Preparation of sodium polysulfide solution<sup>57</sup>

0.58 g of Na<sub>2</sub>S was added to a flask that has been filled with 25 ml distilled water to form a Na<sub>2</sub>S solution. Then 0.72 g of elemental S (sublimed S power) was suspended in the Na<sub>2</sub>S solution and stirred with a magnetic stirrer for about 2 hours at room temperature. The color of the solution changed slowly from pale-yellow to orange with the dissolution of S, and a sodium polysulfide (Na<sub>2</sub>S<sub>*x*</sub>) solution was obtained following the reaction:<sup>57</sup>

$$\text{Na}_2\text{S} + (x - 1) \text{S} \rightarrow \text{Na}_2\text{S}_x$$

### Synthesis of porous CNF–S composites

The novel porous CNF–S composites were prepared by a chemical deposition method in an aqueous solution following the reaction:<sup>57</sup>  $\text{S}_x^{2-} + 2\text{H}^+ \rightarrow (x - 1) \text{S} + \text{H}_2\text{S}$ .

The sublimed S powder and Na<sub>2</sub>S were dissolved in deionized water to form a Na<sub>2</sub>S<sub>*x*</sub> solution as described above. 375 mg of porous CNFs was suspended in 375 ml of NMP and sonicated at 50 °C for 5 h to form a stable porous CNF dispersion. Then, the above-synthesized Na<sub>2</sub>S<sub>*x*</sub> solution was mixed into the porous CNF dispersion in the presence of surfactant cetyl trimethylammonium bromide (CTAB). After 2 hours' sonication and dispersion, these blended solutions were titrated into a 2 mol l<sup>-1</sup> HCOOH solution.<sup>57</sup> The formed CNF–S precipitate was filtered and washed with acetone and distilled water several times in order to eliminate salts and impurities. Finally, these rinsed samples were dried at 50 °C in a drying oven for at least 72 hours.

### Thermal treatment of porous CNF–S composites

The as-synthesized porous CNF–S composites were thermally treated in an Ar environment at 155 °C for 12 h. In order to further decrease the S content, some of the thermally treated samples were further treated at 160 °C for another 6 h.

### Cell assembly and testing

The CNF–S electrodes were prepared by mixing the porous CNF–S composites (including the thermally treated and non-treated porous CNF–S composites), carbon black, and polyvinylidene difluoride (PVDF) at a weight ratio of 70 : 20 : 10 in NMP solvent to form a slurry. The resultant slurry was uniformly spread onto pure aluminium foil using a doctor blade, and dried at 50 °C for 72 hours. CR2032-type coin cells were fabricated by sandwiching a porous polypropylene separator (Celgard 3501, Hoechst Celanese) between the CNF–S electrode and Li metal foil (Cyprus Foote Mineral, 99.98%, USA) in a high-purity Ar-filled glove box. The electrolyte used was 1 M LiTFSI salt per kg of PYR<sub>14</sub>TFSI + PEGDME in a 1 : 1 weight ratio. Cyclic voltammogram (CV) measurements were performed on an AQ4 Gamry Reference 600 electrochemical workstation using a voltage range of 1.0 to 3.6 V vs. Li/Li<sup>+</sup> at a scan rate of 0.05 mV s<sup>-1</sup>. Galvanostatic discharge and charge cycling of the Li/S cells was conducted using an Arbin automatic battery cycler (BT-2000) at several different rates between cut-off potentials of 1.0 and 3.0 V.

### Materials characterization

The samples were characterized using scanning electron microscopy (SEM: Zeiss Gemini Ultra-55), transmission electron microscopy (TEM: Jeol 2100F), energy dispersive X-ray spectroscopy (EDX), thermogravimetric analysis (TGA), X-ray diffraction (XRD) (Diffraktometer D500/501, Siemens), a Brunauer–Emmett–Teller surface area analyzer (BET, Micromeritics ASAP2020), and a Hall effect measurement system (HMS-5000).

### Results and discussion

Fig. 2a–f show SEM images of pure porous CNFs and the porous CNF–S nanocomposites with different S contents after thermal treatments. The pure porous CNFs (Fig. 2a and b) obtained by carbonization of the homogeneous and long electrospun PAN/PMMA bicomponent nanofibers (Fig. S1†) contain a large amount of voids which are also clearly shown in

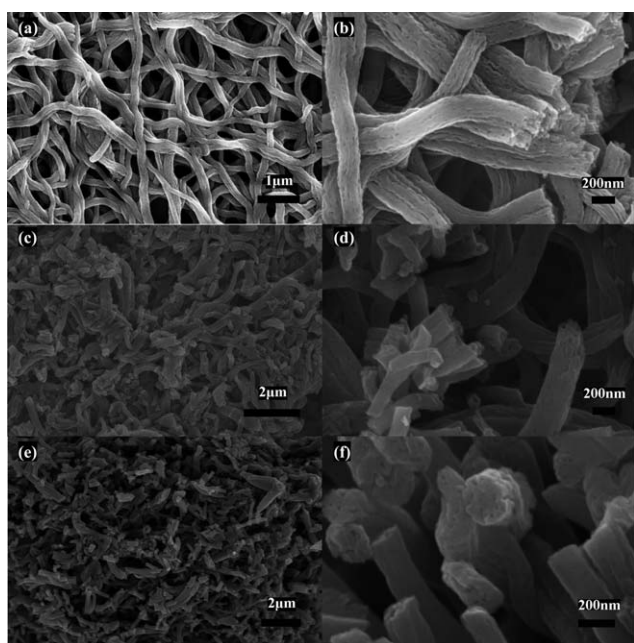


**Fig. 2** SEM images of (a and b) porous CNFs; (c and d) porous CNF-S nanocomposites thermally treated at 155 °C for 12 h; and (e and f) porous CNF-S nanocomposites thermally treated in Ar at 155 °C for 12 h, then at 160 °C for 6 h.

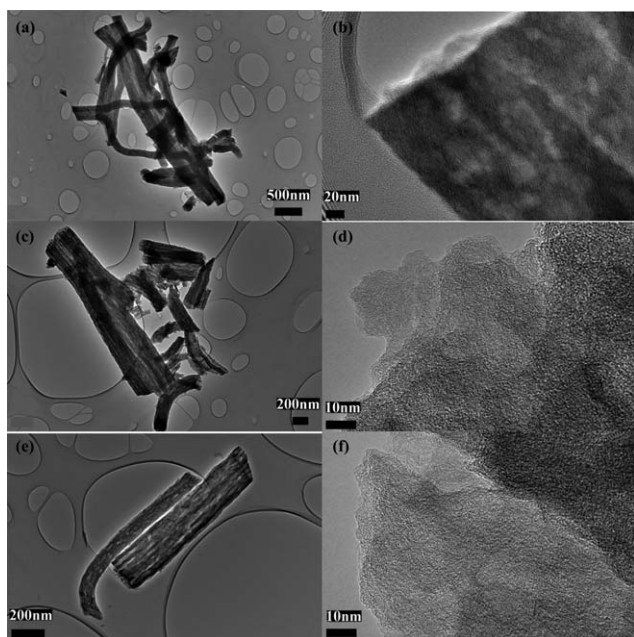


**Fig. 3** TEM images of (a and b) porous CNFs; (c and d) porous CNF-S nanocomposites thermally treated at 155 °C for 12 h; and (e and f) porous CNF-S nanocomposites thermally treated in Ar environment at 155 °C for 12 h, then at 160 °C for 6 h.

the corresponding TEM images in Fig. 3a and b (the large surface area and pore volume are also shown in Table S1 of the ESI†). After the chemical reaction between  $\text{Na}_2\text{S}_x$  and  $\text{HCOOH}$  in the porous CNF-containing microemulsion system, S nanoparticles deposited in the pores of the CNFs. Because of the large

amount of S present, it is unavoidable that some S can also be deposited outside of the pores or attached to the outer surface of the fibers. As a result, the as-prepared porous CNF-S nanocomposites display a non-uniform surface morphology with a convoluted and irregular structure (see SEM images in Fig. S2†) and a high S content of about 76 wt% which denoted full saturation of the micropores (see TEM images in Fig. S3†). In addition, the as-formed porous CNFs are normally several microns long, which may result in discontinuous S loading in some cylindrical pores.<sup>7,26,58</sup> In order to increase the S incorporation into the pores while decreasing the amount of S attached to the fiber surface, the as-prepared porous CNFs-S composite was firstly ball milled to shorten the nanofiber length and then thermally treated at two different temperatures for different times. The corresponding XRD spectra observed from the initially synthesized porous CNF-S nanocomposites and the thermally treated samples are shown in Fig. S4†. The sharp diffraction peaks denote that monoclinic S particles exist in a crystalline state in all of the porous CNF-S nanocomposites before and after the thermal treatments at different temperatures,<sup>57</sup> which are completely different from the XRD pattern of pure CNFs (Fig. S5†). The XRD results also indicate that a portion of the monoclinic sulfur particles are still crystallized on the outer surface of the porous CNFs even after thermal treatment at 155 °C for 12 h, and at the higher temperature of 160 °C for another 6 h.

During the initial thermal treatment at 155 °C for 12 h, part of the bulk S on the external surface of the porous CNFs can melt and diffuse into the pores of the CNFs due to their strong adsorption effects and the high surface areas. As a result, the heat-treated porous CNF-S nanocomposites exhibit a smooth outer surface (Fig. 2c and d). These results indicate that nearly all of the open pores were filled with sulfur (see the TEM images in Fig. 3c and d and the carbon and S elemental maps in Fig. S7a–f† which clearly demonstrate that the S has indeed filled in the pores of the CNFs; also see the surface area and pore volume changes in Table S1 of the ESI†). The TGA results indicate that these thermally treated samples contain about 60 wt% S (Fig. S6†). Further thermal treatment at 160 °C for another 6 h decreased the S content to about 42 wt% (Fig. S6†). The corresponding SEM images in Fig. 2e and f show an uneven surface and undulating surface morphology, and indicate the presence of long, thin interior pores because of the partial evaporation of S from the CNF surfaces or the shallow pores when they were further thermally treated at 160 °C (see the TEM images in Fig. 3e and f, and the corresponding surface area and pore volume values in Table S1 of the ESI†). The residual pore volume in the nanocomposites can provide pathways for electrolyte/ $\text{Li}^+$  entrance and accommodate the active mass volume expansion/contraction during cycling.<sup>10,11</sup>

The thermally treated porous CNF-S nanocomposites with S contents of about 42 wt% and 60 wt% as well as the initially synthesized porous CNF-S nanocomposites before thermal treatment (about 76 wt% S content) were used to prepare electrodes for rechargeable Li/S cells. Fig. 4a presents the CV curves of the porous CNF-S nanocomposite with 42 wt% S. This material shows two main cathodic peaks at about 2.4 and 1.8 V in the first cycle, which can be attributed to the change of S to Li polysulfides and the further reduction of higher-order Li

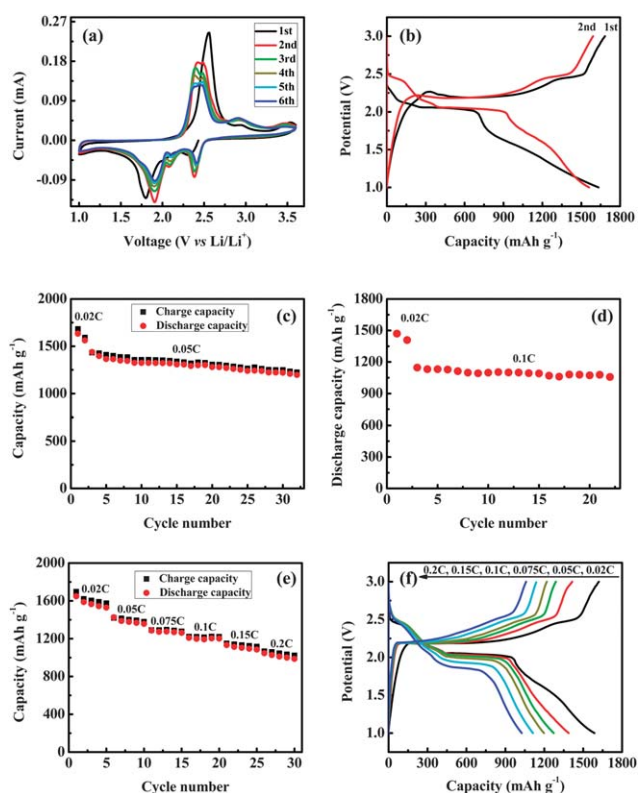


**Fig. 4** (a) CV curve of a porous CNF-S nanocomposite electrode at a  $0.05 \text{ mV s}^{-1}$  scanning rate; (b) galvanostatic charge/discharge profiles of a porous CNF-S nanocomposite electrode at  $0.02 \text{ C}$  rate; (c) cycling performance of a porous CNF-S nanocomposite electrode at a constant rate of (c)  $0.05 \text{ C}$  and (d)  $0.1 \text{ C}$ , after an initial activation processes at  $0.02 \text{ C}$  for 2 cycles; (e and f) reversible capacity vs. current density (rate capability) for porous CNF-S nanocomposite electrodes. All the cells were cycled in the potential window from  $1.0$  to  $3.0 \text{ V}$ . The porous CNF-S nanocomposite electrodes were thermally treated in Ar environment at  $155 \text{ }^\circ\text{C}$  for  $12 \text{ h}$ , then at  $160 \text{ }^\circ\text{C}$  for  $6 \text{ h}$ . The S content is  $42 \text{ wt}\%$  in the CNF-S nanocomposite (the overall S content, including additives and binders in the electrode is about  $29.4 \text{ wt}\%$ ).

polysulfides to Li sulfides, respectively.<sup>8,10,13,19,20,26,31,36,38,47,60</sup> In the first anodic scan, the two expected oxidation peaks overlap and form one large peak at about  $2.55 \text{ V}$ . This overlap may be because of high overvoltage for conversion of  $\text{Li}_2\text{S}$  to Li polysulfide.<sup>19</sup> In the subsequent scans, the main reduction peaks are shifted to higher potentials and the oxidation peaks to lower potentials, indicating an improvement of reversibility of the electrode with cycling. In addition, as the cycle number increased, it is observed that the oxidation peak at  $2.55 \text{ V}$  becomes less significant, while another new one at  $2.4 \text{ V}$  grows higher in intensity. There is also another new reduction peak at around  $2.1 \text{ V}$ . The CV results indicate that our porous CNFs have an excellent conductive structure in which the electrochemically active S is well dispersed and in good contact with the carbon matrix. The porous carbon matrix also has a strong adsorbing ability to suppress the dissolution of the polysulfides into the electrolyte during the discharge/charge process.

In order to further investigate the electrochemical performance of the porous CNF-S nanocomposite with  $42 \text{ wt}\%$  S, we carried out galvanostatic cycling performance and rate capability

evaluations in coin cells with Li metal as the anode. All of the capacity values in this article are calculated according to the mass of S. The typical discharge/charge profiles for the initial two cycles at the  $0.02 \text{ C}$  rate ( $1 \text{ C} = 1675 \text{ mA g}^{-1}$ ) between  $1.0$  and  $3.0 \text{ V}$  are presented in Fig. 4b. The discharge curves show two plateaus, which can be assigned to the two step reaction of S with Li during the discharge process, as demonstrated in CV measurement.<sup>8,10,13,19,20,26,31,36,38,47,60</sup> Further cycling tests show that the electrode prepared from the porous CNF-S nanocomposite with  $42 \text{ wt}\%$  S also exhibits stable cycling for at least 30 cycles and rate capability up to at least  $0.2 \text{ C}$ . Fig. 4c illustrates the stable cycling of a coin cell at  $0.05 \text{ C}$  after the initial two cycles' activation process at  $0.02 \text{ C}$ . The initial activation cycles at low rates can achieve improved reversibility, as indicated in the cyclic voltammograms, and help the Li/S cells approach the maximum sulfur utilization. The porous CNF-S nanocomposite electrode can deliver a discharge capacity of about  $1439 \text{ mA h g}^{-1}$  at the first cycle at  $0.05 \text{ C}$ , with a corresponding coulombic efficiency of about  $100\%$ . After the initial cycles, the porous CNF-S nanocomposite electrode displays electrochemical reversibility with a discharge capacity of  $1396 \text{ mA h g}^{-1}$  at the 2<sup>nd</sup> cycle at  $0.05 \text{ C}$ . Even at the 30<sup>th</sup> cycle at  $0.05 \text{ C}$ , the reversible capacity remains at about  $1220 \text{ mA h g}^{-1}$ , indicating about  $85\%$  capacity retention. In addition, the coulombic efficiency can be maintained in the range of  $97\text{--}98\%$ . The reversibility indicates that porous CNF materials can provide an effective electron conduction path and their network-like structure forms a stable structure for the S electrode.

In another experiment, a Li/S coin cell was operated at a higher rate of  $0.1 \text{ C}$  after the initial activation processes at a low rate of  $0.02 \text{ C}$  (Fig. 4d). Although the discharge capacity decreased to about  $1146 \text{ mA h g}^{-1}$  upon the initial cycling at  $0.1 \text{ C}$ , the capacity then remained constant at about  $1057 \text{ mA h g}^{-1}$  for 20 cycles ( $92\%$  capacity retention). We attribute the significantly enhanced electrochemical performance to the specially designed nanostructure which comes from our unique chemical reaction-deposition strategy. These special reaction systems can provide a distinctive microenvironment for the formation of non-aggregated and uniform S nanoparticles,<sup>57</sup> which are directly deposited on porous CNFs in the subsequent chemical reactions (including various kinds of pore volumes and also the surface). The highly dispersed S in the porous CNF-S nanocomposite can successfully accommodate the volume change associated with the Li/S electrochemical reactions. The large specific surface area and the uniform mesoporous channels in the nanocomposite can restrict the diffusion of the polysulfides during the discharge/charge process. In addition, the chemical reaction-deposition strategy provides assuredly intimate contact between the S and the CNFs (this would be impossible for the simple ball milling and thermal treatment processes). The intimate contact of the nano-dispersed S within the porous CNFs ensures a good electrical path to the active S and improves the S utilization.

The rate capability of our porous CNF-S electrode is demonstrated in Fig. 4e and f. The reversible capacity at a low rate of  $0.05 \text{ C}$  is about  $1400 \text{ mA h g}^{-1}$  after the initial discharge process at  $0.02 \text{ C}$ . This coin cell shows a reversible capacity of  $987 \text{ mA h g}^{-1}$  at a rate of  $0.2 \text{ C}$  ( $335 \text{ mA g}^{-1}$ ) after being continuously cycled for 30 cycles at various rates, owing to the good electrical conductivity of the porous CNFs as a matrix for the insulating S.<sup>8,10,13,19,20,26,31,36,38,47,60</sup>

The electrochemical performance of the porous CNF-S nanocomposite electrodes with higher S contents was also explored. The CV curve of the porous CNF-S nanocomposite with 60 wt% S shows that the higher S content samples have a small reduction peak position shift after the first cycle (at  $\sim 1.75$  V and 2.35 V). There is also one anodic peak at about 2.60 V, shifting slightly to lower voltage with increase in cycle number, although the shape is nearly the same as that for the first cycle (Fig. S8a†). These differences compared with the results for the porous CNF-S nanocomposite with lower S content (42 wt%) can be ascribed to the lower S utilization and reduced reversibility of the porous CNF-S nanocomposite electrodes with higher S content. The nanocomposite with 60 wt% S had an initial discharge capacity of  $1125 \text{ mA h g}^{-1}$  at 0.05 C after the two cycle activation process at 0.02 C (see initial two cycles' discharge/charge profiles at 0.02 C in Fig. S8b†). This value decreases to  $709 \text{ mA h g}^{-1}$  after 30 cycles (63% capacity retention) (Fig. S8c†). In addition, these porous CNF-S nanocomposite electrodes also have high reversible capacity and relatively stable cycling for at least 30 cycles at higher rates, as shown in Fig. S8d and e†. For the porous CNF-S nanocomposite with 76 wt% S (the samples before thermal treatment), the utilization of the S is much lower (Fig. S9†). This may be caused by the full saturation of the micropores with S in the porous CNFs, which may prevent good access by both the electrolyte and electrons.<sup>7,10</sup> Therefore, the high dispersion of elemental S inside the narrow micropores of CNFs is critical for achieving the high rate discharge capability of the S electrode.

Importantly, the narrow micropores of the CNFs can trap elemental S and Li polysulfides during cycling due to their strong adsorption, preventing the shuttle mechanism, mass loss of the active materials and the formation of a  $\text{Li}_2\text{S}$  insulating layer on the composite surface. The fact that the electrochemical reaction can be constrained mainly to the insides of the narrow micropores is responsible for the enhancement of the improved electrochemical stability of the S electrode. In addition to the above-mentioned advantages, these porous CNF-S nanocomposites can also provide intimate electrical contact, and decrease the transport distances of both Li ions and electrons, while greatly increasing their transport rates. Therefore, the high dispersion of elemental S inside the narrow micropores of CNFs (which comes from our unique chemical reaction-deposition method) is beneficial to improvement of the discharge capacity and capacity retention in the S electrode by enhancement of electrical contact and retention of Li polysulfides. In addition, as was previously reported, the selection of a suitable electrolyte is also indispensable in the successful utilization of the active material in Li/S cells because of the multi-step reduction reactions of S and the variations in the solubility of the different polysulfides in the electrolyte.<sup>10,36,39,40,60</sup> The electrolyte should satisfy a number of requirements such as high ionic conductivity, low polysulfide solubility, low viscosity, electrochemical stability, chemical stability towards Li and safety. In our experiments, an ionic liquid-based electrolyte  $\text{PYR}_{14}\text{TFSI-LiTFSI-PEGDME}$  mixture was used. This electrolyte has suitable viscosity, chemical stability and ionic conductivity.<sup>8,36,37</sup> It also can reduce the solubility of polysulfides in the electrolyte, maintain a more stable capacity and improve rate performance.

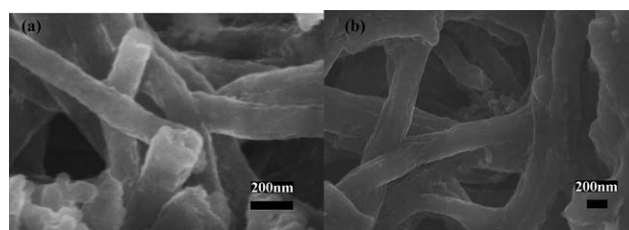


**Fig. 5** SEM images of a porous CNF-S nanocomposite electrode after 30 charge/discharge cycles at a constant rate of 0.05 C.

To demonstrate the role of CNFs as a strong mechanical framework to maintain electrode integrity, we also explored the morphology and structural changes of the porous CNF-S electrodes after repeated Li insertion/extraction. The coin cell electrochemically evaluated at 0.05 C for 30 cycles was disassembled and characterized by SEM. The results are displayed in Fig. 5. Comparing Fig. 2e and f before cycling to Fig. 5, it was found that the original porous nanofibrous morphology and structure clearly were retained after cycling.

In conclusion, we have prepared porous CNF-S nanocomposites in a controllable fashion through simple and convenient carbonization of electrospun PAN/PMMA bi-component nanofibers and the subsequent chemical reaction-deposition strategy. These porous CNF-S nanocomposites were used as electrodes for rechargeable Li/S cells to evaluate their electrochemical performance. The results show that the highly electronically conductive porous CNFs provide an extremely high surface area to adsorb and disperse S and ameliorate its disadvantages, such as the insulating nature of S and the solubility of polysulfide intermediates in organic solvent based electrolytes. The porous CNF-S nanocomposite with 42 wt% S can deliver nearly  $1400 \text{ mA h g}^{-1}$  initial discharge capacity at the 0.05 C rate, with 85% capacity retention after 30 discharge/charge cycles, reflecting a relatively stable reversible capacity and improved capacity retention. In addition, when measured at higher rates, the nanocomposite electrode also exhibits clearly improved cyclability ( $1057 \text{ mA h g}^{-1}$  after 20 cycles at 0.1 C) and rate capability ( $987 \text{ mA h g}^{-1}$  at 0.2 C after 30 cycles at various rates). It should be noted that the experimental conditions, such as the ratios of PAN and PMMA phases and their types in the electrospinning, the thermal treatment temperatures, *etc.*, can be optimized in order to improve the surface areas and the pore volumes of the as-prepared porous CNFs and so to control the S loading and the final S utilizations in porous CNF-S composites to further improve electrochemical performance when used as electrodes in Li/S cells.

## Acknowledgements

This work was partially supported by the Office of Science, Office of Basic Energy Sciences, of the U. S. Department of Energy under contract no. DE-AC02-05CH11231. M.R. was partially supported by the China Scholarship Council while visiting the Department of Chemical & Biomolecular Engineering at UC Berkeley. The authors would like to thank Virginia Altoe, Tevye Kuykendall, Yanbo Fu and Vincent Battaglia for their assistance in experiments.

## Notes and references

- 1 P. G. Bruce, B. Scrosati and J.-M. Tarascon, *Angew. Chem., Int. Ed.*, 2008, **47**, 2930–2946.
- 2 L. Ji, Z. Lin, M. Alcoutlabi and X. Zhang, *Energy Environ. Sci.*, 2011, **4**, 2682–2699.
- 3 H. Li, Z. Wang, L. Chen and X. Huang, *Adv. Mater.*, 2009, **21**, 4593–4607.
- 4 A. Manthiram, A. Vadivel Murugan, A. Sarkar and T. Muraliganth, *Energy Environ. Sci.*, 2008, **1**, 621–638.
- 5 J. B. Goodenough and Y. Kim, *Chem. Mater.*, 2010, **22**, 587–603.
- 6 S. W. Lee, B. M. Gallant, H. R. Byon, P. T. Hammond and Y. Shao-Horn, *Energy Environ. Sci.*, 2011, **4**, 1972–1985.
- 7 X. Ji and L. F. Nazar, *J. Mater. Chem.*, 2010, **20**, 9821–9826.
- 8 J. Shim, K. A. Striebel and E. J. Cairns, *J. Electrochem. Soc.*, 2002, **149**, A1321–A1325.
- 9 X.-P. Gao and H.-X. Yang, *Energy Environ. Sci.*, 2010, **3**, 174–189.
- 10 B. Zhang, X. Qin, G. R. Li and X. P. Gao, *Energy Environ. Sci.*, 2010, **3**, 1531–1537.
- 11 X. Ji, K. T. Lee and L. F. Nazar, *Nat. Mater.*, 2009, **8**, 500–506.
- 12 B. Jin, J.-U. Kim and H.-B. Gu, *J. Power Sources*, 2003, **117**, 148–152.
- 13 S. Wei, H. Zhang, Y. Huang, W. Wang, Y. Xia and Z. Yu, *Energy Environ. Sci.*, 2011, **4**, 736–740.
- 14 J. Hassoun and B. Scrosati, *Angew. Chem., Int. Ed.*, 2010, **49**, 2371–2374.
- 15 D. Liu and G. Cao, *Energy Environ. Sci.*, 2010, **3**, 1218–1237.
- 16 V. Etacheri, R. Marom, R. Elazari, G. Salitra and D. Aurbach, *Energy Environ. Sci.*, 2011, **4**, 3243–3262.
- 17 Y. Yang, M. T. McDowell, A. Jackson, J. J. Cha, S. S. Hong and Y. Cui, *Nano Lett.*, 2010, **10**, 1486–1491.
- 18 C. Liang, N. J. Dudney and J. Y. Howe, *Chem. Mater.*, 2009, **21**, 4724–4730.
- 19 Y. Cao, X. Li, I. A. Aksay, J. Lemmon, Z. Nie, Z. Yang and J. Liu, *Phys. Chem. Chem. Phys.*, 2011, **13**, 7660–7665.
- 20 N. Jayaprakash, J. Shen, S. S. Moganty, A. Corona and L. A. Archer, *Angew. Chem., Int. Ed.*, 2011, **50**, 5904–5908.
- 21 D. Deng, M. G. Kim, J. Y. Lee and J. Cho, *Energy Environ. Sci.*, 2009, **2**, 818–837.
- 22 G. Jeong, Y.-U. Kim, H. Kim, Y.-J. Kim and H.-J. Sohn, *Energy Environ. Sci.*, 2011, **4**, 1986–2002.
- 23 V. Kolosnitsyn and E. Karaseva, *Russ. J. Electrochem.*, 2008, **44**, 506–509.
- 24 K. Kumaresan, Y. Mikhaylik and R. E. White, *J. Electrochem. Soc.*, 2008, **155**, A576–A582.
- 25 J. R. Akridge, Y. V. Mikhaylik and N. White, *Solid State Ionics*, 2004, **175**, 243–245.
- 26 L. Yuan, H. Yuan, X. Qiu, L. Chen and W. Zhu, *J. Power Sources*, 2009, **189**, 1141–1146.
- 27 L. Yin, J. Wang, J. Yang and Y. Nuli, *J. Mater. Chem.*, 2011, **21**, 6807–6810.
- 28 X. He, W. Pu, J. Ren, L. Wang, J. Wang, C. Jiang and C. Wan, *Electrochim. Acta*, 2007, **52**, 7372–7376.
- 29 C. Wang, J. Chen, Y. Shi, M. Zheng and Q. Dong, *Electrochim. Acta*, 2010, **55**, 7010–7015.
- 30 S.-R. Chen, Y.-P. Zhai, G.-L. Xu, Y.-X. Jiang, D.-Y. Zhao, J.-T. Li, L. Huang and S.-G. Sun, *Electrochim. Acta*, 2011, DOI: 10.1016/j.electacta.2011.03.005, in press.
- 31 C. Lai, X. P. Gao, B. Zhang, T. Y. Yan and Z. Zhou, *J. Phys. Chem. C*, 2009, **113**, 4712–4716.
- 32 B. Zhang, C. Lai, Z. Zhou and X. P. Gao, *Electrochim. Acta*, 2009, **54**, 3708–3713.
- 33 F. Wu, J. Chen, R. Chen, S. Wu, L. Li, S. Chen and T. Zhao, *J. Phys. Chem. C*, 2011, **115**, 6057–6063.
- 34 M. Sun, S. Zhang, T. Jiang, L. Zhang and J. Yu, *Electrochem. Commun.*, 2008, **10**, 1819–1822.
- 35 J. Wang, J. Yang, J. Xie and N. Xu, *Adv. Mater.*, 2002, **14**, 963–965.
- 36 J. H. Shin and E. J. Cairns, *J. Power Sources*, 2008, **177**, 537–545.
- 37 D. Marmorstein, T. H. Yu, K. A. Striebel, F. R. McLarnon, J. Hou and E. J. Cairns, *J. Power Sources*, 2000, **89**, 219–226.
- 38 J. Wang, S. Y. Chew, Z. W. Zhao, S. Ashraf, D. Wexler, J. Chen, S. H. Ng, S. L. Chou and H. K. Liu, *Carbon*, 2008, **46**, 229–235.
- 39 T. Kobayashi, Y. Imade, D. Shishihara, K. Homma, M. Nagao, R. Watanabe, T. Yokoi, A. Yamada, R. Kanno and T. Tatsumi, *J. Power Sources*, 2008, **182**, 621–625.
- 40 L. X. Yuan, J. K. Feng, X. P. Ai, Y. L. Cao, S. L. Chen and H. X. Yang, *Electrochem. Commun.*, 2006, **8**, 610–614.
- 41 S.-E. Cheon, S.-S. Choi, J.-S. Han, Y.-S. Choi, B.-H. Jung and H. S. Lim, *J. Electrochem. Soc.*, 2004, **151**, A2067–A2073.
- 42 J.-W. Choi, J.-K. Kim, G. Cheruvally, J.-H. Ahn, H.-J. Ahn and K.-W. Kim, *Electrochim. Acta*, 2007, **52**, 2075–2082.
- 43 S. S. Jeong, Y. T. Lim, Y. J. Choi, G. B. Cho, K. W. Kim, H. J. Ahn and K. K. Cho, *J. Power Sources*, 2007, **174**, 745–750.
- 44 D. Aurbach, E. Pollak, R. Elazari, G. Salitra, C. S. Kelley and J. Affinito, *J. Electrochem. Soc.*, 2009, **156**, A694–A702.
- 45 J.-W. Choi, G. Cheruvally, D.-S. Kim, J.-H. Ahn, K.-W. Kim and H.-J. Ahn, *J. Power Sources*, 2008, **183**, 441–445.
- 46 X. Yu, J. Xie, J. Yang and K. Wang, *J. Power Sources*, 2004, **132**, 181–186.
- 47 Y. Jung and S. Kim, *Electrochem. Commun.*, 2007, **9**, 249–254.
- 48 J. Sun, Y. Huang, W. Wang, Z. Yu, A. Wang and K. Yuan, *Electrochim. Acta*, 2008, **53**, 7084–7088.
- 49 F. Croce, M. L. Focarete, J. Hassoun, I. Meschini and B. Scrosati, *Energy Environ. Sci.*, 2011, **4**, 921–927.
- 50 V. Thavasi, G. Singh and S. Ramakrishna, *Energy Environ. Sci.*, 2008, **1**, 205–221.
- 51 S. Chen, H. Hou, F. Harnisch, S. A. Patil, A. A. Carmona-Martinez, S. Agarwal, Y. Zhang, S. Sinha-Ray, A. L. Yarin, A. Greiner and U. Schroder, *Energy Environ. Sci.*, 2011, **4**, 1417–1421.
- 52 L. Ji, Z. Lin, A. J. Medford and X. Zhang, *Chem.–Eur. J.*, 2009, **15**, 10718–10722.
- 53 L. Ji, Z. Lin, B. Guo, A. J. Medford and X. Zhang, *Chem.–Eur. J.*, 2010, **16**, 11543–11548.
- 54 Z. Lin, L. Ji, M. D. Woodroof, Y. Yao, W. Krause and X. Zhang, *J. Phys. Chem. C*, 2010, **114**, 3791–3797.
- 55 L. Ji, Z. Lin, A. J. Medford and X. Zhang, *Carbon*, 2009, **47**, 3346–3354.
- 56 L. Ji, Z. Lin, R. Zhou, Q. Shi, O. Toprakci, A. J. Medford, C. R. Millns and X. Zhang, *Electrochim. Acta*, 2010, **55**, 1605–1611.
- 57 Y.-M. Guo, Y.-H. Deng, J.-Z. Zhao and Z.-C. Wang, *Chin. J. Chem.*, 2005, **63**, 337–340.
- 58 Y.-J. Choi, K.-W. Kim, H.-J. Ahn and J.-H. Ahn, *J. Alloys Compd.*, 2008, **449**, 313–316.
- 59 C. Kim, Y. I. Jeong, B. T. N. Ngoc, K. S. Yang, M. Kojima, Y. A. Kim, M. Endo and J.-W. Lee, *Small*, 2007, **3**, 91–95.
- 60 S. Kim, Y. Jung and S.-J. Park, *Electrochim. Acta*, 2007, **52**, 2116–2122.